PHYSICAL REVIEW C **81**, 044605 (2010)

Elastic scattering and total reaction cross section of ^{6}He + ^{120}Sn

P. N. de Faria,[1] R. Lichtenthäler,[1] K. C. C. Pires,[1] A. M. Moro,[2] A. Lépine-Szily,[1] V. Guimarães,[1] D. R. Mendes Jr.,[1] A. Arazi,[3] M. Rodríguez-Gallardo,[2,4] A. Barioni,[1] V. Morcelle,[1] M. C. Morais,[1] O. Camargo Jr.,[1] J. Alcantara Nuñez,[1] and M. Assunção[5]

[1]*Instituto de Fisica-Universidade de São Paulo, C. P. 66318, 05389-970 São Paulo, SP, Brazil*
[2]*Departamento de FAMN, Universidad de Sevilla, Apartado 1065, E-41080 Sevilla, Spain*
[3]*Laboratorio Tandar, Comisión Nacional de Energía Atómica, Av. del Libertador 8250, 1429 Buenos Aires, Argentina*
[4]*Instituto de Estructura de la Materia, CSIC, Serrano 123, E-28006 Madrid, Spain*
[5]*Universidade Federal de São Paulo, Campus Diadema, 09941-510 São Paulo, SP, Brazil*

(Received 23 December 2009; published 16 April 2010)

The elastic scattering of ^{6}He on ^{120}Sn has been measured at four energies above the Coulomb barrier using the ^{6}He beam produced at the RIBRAS (Radioactive Ion Beams in Brasil) facility. The elastic angular distributions have been analyzed with the optical model and three- and four-body continuum-discretized coupled-channels calculations. The total reaction cross sections have been derived and compared with other systems of similar masses.

DOI: 10.1103/PhysRevC.81.044605 PACS number(s): 25.60.Bx, 24.10.Eq, 24.10.Ht, 25.70.Bc

I. INTRODUCTION

Reactions induced by light exotic projectiles at low energies are a very interesting subject that has not yet been fully explored. Light nuclei far from the stability valley such as ^{6}He, ^{8}B, and others have one or more nucleons loosely bound to a core forming a halo or a skinlike structure with densities much lower than those of normal nuclear matter. Due to the small binding energies and low angular momenta of these valence nucleons their wave functions usually extend over large distances from the core and, as a consequence, these projectiles can easily deform and break up during collision with a target, affecting the imaginary part of the potential and enhancing the total reaction cross section. The first experiments using light exotic projectiles at low energies have been performed for heavy targets such as ^{6}He + ^{209}Bi and ^{208}Pb [1–4] and new interesting phenomena, such as the damping of the Fresnel diffraction peak in the elastic angular distribution and very large total reaction cross sections, have been reported. Despite the uncertainties involved in the optical model (OM) analysis of the elastic angular distributions, the existence of a larger total reaction cross section for ^{6}He + X systems in comparison with other stable projectiles is clear. The behavior of the total reduced reaction cross section as a function of the reduced energy for several stable and exotic projectiles [5,6] on medium-mass targets has revealed a much higher total reaction cross section for the ^{6}He + ^{64}Zn system as compared to other weakly bound and tightly bound stable projectiles. Similar observations have been performed recently for the proton-rich ^{8}B nucleus on ^{58}Ni [7], for which a very large reduced total reaction cross section has been observed in comparison with other reactions induced by weakly bound projectiles, such as ^{6}Li + ^{58}Ni and ^{7}Be + ^{58}Ni.

An important step in this study is to identify the reaction channels responsible for the increase of the reaction cross section of exotic systems. The projectile breakup and, more recently, the neutron transfer reactions have been identified as important reaction channels in collisions induced by the neutron-rich ^{6}He projectile. Measurement of elastic scattering of exotic projectiles on several mass targets could shed some light on this question. In particular, the role of the Coulomb and nuclear breakup processes and their interference are important issues that could be clarified by the systematic measurement of elastic scattering of exotic nuclei on several targets.

An additional interesting aspect of elastic-scattering studies involving ^{6}He, is that the projectile consists of an α core plus two neutrons forming a bound three-body Borromean system. Theoretical efforts have been made to calculate three-body wave functions for ^{6}He and only very recently are powerful four-body continuum-discretized coupled-channels (CDCC) programs being developed to take into account such effects on the elastic scattering and in the breakup channel [8–10]. Experimental data of the elastic scattering at low energies are thus welcome to compare with the predictions of those calculations.

In this work we present new data of the medium-heavy mass system ^{6}He + ^{120}Sn. We measured four elastic-scattering angular distributions at energies $E_{\rm lab}$ = 17.4, 18.05, 19.8, and 20.5 MeV, the Coulomb barrier being estimated around $E_{\rm CB}^{\rm lab} \approx$ 15.9 MeV. This article is structured as follows. In Sec. II we describe the experimental setup used in this experiment and outline the main steps of the data analysis. In Sec. III the measured elastic angular distributions are compared with the OM and CDCC calculations, and we discuss the total reaction cross section extracted from both procedures. Finally, we present a systematics of the total reaction cross section for systems with exotic ^{6}He, weakly bound ^{6,7}Li, and tightly bound ^{4}He projectiles on medium-heavy mass ^{120}Sn and ^{138}Ba targets. In Sec. IV, the main conclusions of this work are summarized.

II. EXPERIMENTAL SETUP AND RESULTS

The experiment was performed in the 8UD São Paulo Pelletron Laboratory using the RIBRAS (Radioactive Ion Beams in Brazil) system [11,12] (see Fig. 1). The ^{7}Li^{3+} primary beam of energies in the range $E_{\rm lab}$ = 24–26 MeV

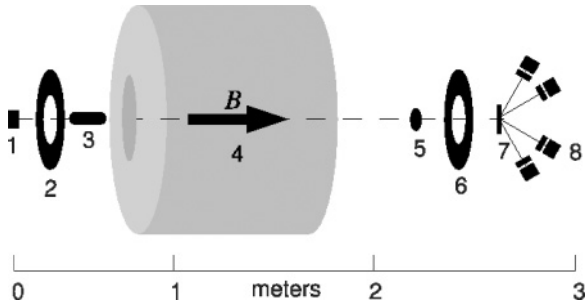

FIG. 1. Schematic view of the RIBRAS system (see text for details).

and intensities of about 300 nAe was focused on a 12μ ^{9}Be foil (labeled "1" in Fig. 1). The first collimator (2) and the Faraday cup (3) just after the primary target define the acceptance angular range of the solenoid (4) which is presently between 2° and 6°. The Faraday cup prevents the primary beam from entering into the solenoid and measures its intensity, which is integrated during each run. The ^{6}He beam was produced by the ^{9}Be(^{7}Li,^{6}He)^{10}B transfer reaction and was focused by the solenoid in the secondary target (7) position. The primary beam particles (^{7}Li^{3+} elastically scattered by the primary target) have less magnetic rigidity and thus they are focused before the secondary target. To suppress them, a "lollipop" (5) is placed at that position. The ^{6}He production rate was maximized in the beginning of the experiment by varying the solenoid current and measuring the ^{6}He particles elastically scattered by a gold secondary target. During the experiment the ^{6}He beam intensities were around 10^{4}–10^{5} pps at the secondary-target position. A 3.8 mg/cm^2 ^{120}Sn (98.29%) target and a 3 mg/cm^2 ^{197}Au target were mounted in the secondary scattering chamber (7). The gold target was used for normalization purposes because the ^{6}He + ^{197}Au scattering is pure Rutherford at the energies and angular range of the experiment. A system of four ΔE (20 μm)-E (1000 μm) silicon telescopes was mounted in a rotating plate inside the secondary chamber to perform angular distribution measurements. The detectors have effective areas of 150 mm^2 (at forward angles) and 300 mm^2 (at backward angles) and the detection solid angles are in the range 10–20 msr. In Fig. 2 we present two ΔE-E_{total} spectra with gold and tin targets where $E_{\text{total}} = E + \Delta E$. We clearly see the ^{6}He peak separated from the ^{7}Li^{2+} and α-particle contaminants. The energy resolution of the ^{6}He beam was of about 1 MeV mainly due to the energy straggling in the primary target. The elastic-scattering cross section can be determined by the expression below, normalized by the gold target run,

$$\sigma_{\text{cm}}^{^{6}\text{He}+^{120}\text{Sn}}(\theta) = \frac{N_c^{\text{Sn}}}{N_c^{\text{Au}}}\frac{N_b^{\text{Au}}}{N_b^{\text{Sn}}}\frac{N_t^{\text{Au}}}{N_t^{\text{Sn}}}\frac{J^{\text{Sn}}}{J^{\text{Au}}}\sigma_{\text{cm}}^{^{6}\text{He}+^{197}\text{Au}}(\theta), \qquad (1)$$

where N_c is the area of the peak of interest, J is the factor of transformation from the laboratory to the center-of-mass system, N_b is the total number of ^{6}He beam particles during the run, and N_t is the surface density of the target in number of atoms/cm^2. This expression has the advantage of being independent of the detection solid angles. The ratio $N_b^{\text{Au}}/N_b^{\text{Sn}}$ is taken as the ratio of the integrators of the runs with gold and tin targets. We performed runs with the gold target before and after every run with the tin target to monitor the production rate during the whole experiment.

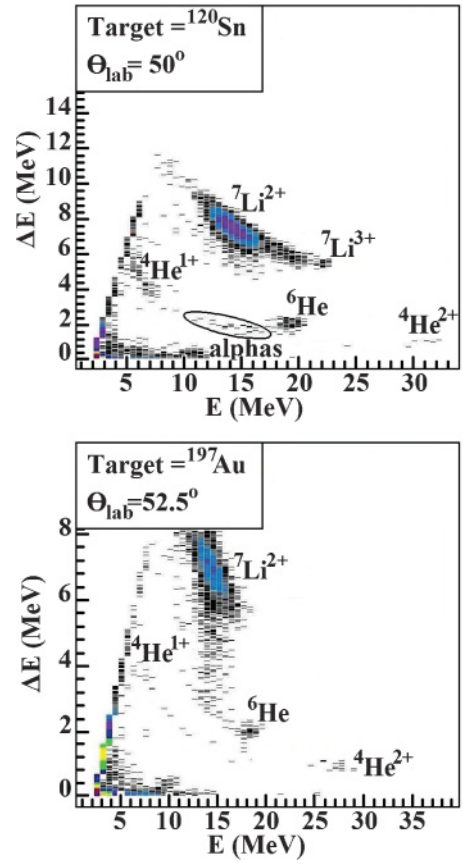

FIG. 2. (Color online) Biparameteric spectra recorded for the tin target (top) and the gold target (bottom).

The ^{6}He + ^{120}Sn elastic angular distributions are presented in Fig. 3. The energies indicated in the labels take into account the energy loss in the tin target and hence they actually correspond to the estimated ^{6}He energy in the middle of the target.

III. ANALYSIS OF THE ELASTIC SCATTERING

A. Optical model analysis

As a first step in the analysis we performed OM calculations using the SFRESCO code [13]. A Woods-Saxon shape was used and the six parameters were varied freely to fit the experimental data. Initially, the four angular distributions were analyzed altogether using a single set of potential parameters. This procedure can be justified by the relatively small energy interval of the measurements and the small number of points in each angular distribution. The global Woods-Saxon parameters obtained are $V_0 = 216.3$ MeV, $r_{0r} = 0.90$ fm, $a_r = 0.90$ fm, $W = 12.42$ MeV, $r_{0_i} = 1.42$ fm, and $a_i = 0.75$ fm, where $R = r_0(A_p^{1/3} + A_t^{1/3})$. In a second step we started the search from these parameters and let V, r_{or}, and the imaginary strength W vary freely for each energy.

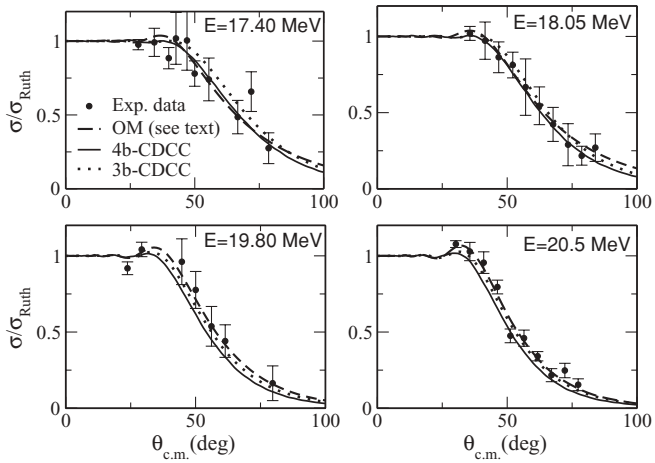

FIG. 3. ^{6}He + ^{120}Sn elastic angular distributions. The experimental data of this experiment (solid circles) are compared with OM (dashed lines), three-body CDCC (dotted lines), and four-body CDCC (solid lines) calculations. See text for details.

The fits are shown in Fig. 3 by dashed lines and the final OM parameters are presented in Table I. The OM total reaction cross sections are listed in the second column of Table II. During the OM analysis we observed that different potential parameters reproduced equally well the data, indicating the presence of a large ambiguity in the Woods-Saxon parameters. The large imaginary radius and diffuseness compared to the real part indicate the need for a long-range absorptive term in the interacting potential.

A remarkable feature of the best potential (Table I) is that the imaginary part decreases with increasing energy while the real part increases. A similar behavior, known as the breakup threshold anomaly, has been reported previously [14,15] in weakly bound systems.

B. CDCC calculations

Theoretically, the effect of the coupling to breakup states can be described explicitly within the CDCC framework [16]. The method was first developed for three-body (3b-CDCC) problems (two-body projectile plus a target) and it has been successfully used for many reactions induced by stable and exotic weakly bound nuclei (e.g., Refs. [4,17]).

The first applications of this method to ^{6}He-induced reactions [1,2] made use of a simple two-body model ($\alpha + 2n$) of the ^{6}He nucleus (the so-called dineutron model)

TABLE I. Woods-Saxon optical potential parameters for the ^{6}He + ^{120}Sn system. The values of $r_{0i} = 1.42$ fm, $a_i = 0.75$ fm, and $a_r = 0.90$ fm were kept fixed for all the energies (see text for more details). $R = r_0(A_p^{1/3} + A_t^{1/3})$ and $r_c = 0.8$ fm.

$E_{\rm lab}$ (MeV)	V (MeV)	r_{0r} (fm)	W (MeV)
17.40	10	0.37	19.4
18.05	62	0.45	13.8
19.80	176	0.75	6.70
20.50	214	0.75	6.90

in which the α-$2n$ interaction is parametrized with some simple form (typically a Woods-Saxon shape) whose depth is adjusted to reproduce the experimental two-neutron separation energy, $\varepsilon_b = -0.97$ MeV. However, this model is known to overestimate the radial extension of the ground-state wave function and, consequently, the couplings to the continuum. A possible improvement of this approach, proposed in Ref. [18], is to define an effective α-$2n$ separation energy, which is adjusted to reproduce the rms radius predicted within a more realistic three-body model. This procedure leads to an effective binding energy around $\varepsilon_b = -1.6$ MeV. This improved dineutron model has been found to reproduce satisfactorily the elastic-scattering data of several ^{6}He-induced reactions [18].

Continuum states with $j^\pi = 0^+$, 1^-, 2^+, 3^-, and 4^+ were included. The $2n$-α interaction was adopted from Ref. [18]. For the 0^+ states, the depth of this potential was adjusted to reproduce the separation energy of 1.6 MeV, whereas for 2^+ states the depth was adjusted to give a resonance at an excitation energy of 1.8 MeV. For 1^- we just adopted the depth found for the ground state. The $2n$-^{120}Sn and α-^{120}Sn interactions, which are required to generate the projectile-target coupling potentials, were taken from the deuteron global potential of Lohr and Haeberli [19] and the α potential of Tabor *et al.* [20], respectively.

The calculations were performed with the code FRESCO [13]. The results of these calculations are shown in Fig. 3 (dotted lines). Overall, they reproduce the data at the different energies reasonably well.

Despite the success of the dineutron model, a proper treatment of the reactions induced by Borromean nuclei, like ^{6}He, requires a four-body formalism (three-body projectile plus a target). Recently the CDCC framework has been extended to four-body (4b-CDCC) problems [8–10]. In this work we use the four-body CDCC formalism developed in Ref. [9] to calculate the elastic angular distributions for the measured reaction. To discretize the three-body continuum we use a pseudo-state (PS) method, the transformed harmonic oscillator (THO) method [21] (already used within the four-body CDCC formalism in Ref. [9]). The discretization methods based on PS consists in representing the continuum spectrum of the projectile by the eigenstates obtained upon diagonalization of the projectile Hamiltonian in a truncated basis of square-integrable basis (PS basis).

Here we use the same structure model for the three-body system ^{6}He(α + n + n), as in Refs. [9,21]. The Hamiltonian includes two-body potentials plus an effective three-body potential. The ^{6}He ground-state wave function ($j = 0^+$) needed to construct the THO basis is generated using the codes FACE [22] and STURMXX [23]. The maximum hypermomentum used was $K_{\rm max} = 8$. The parameters of the three-body interaction are adjusted to reproduce the ground-state separation energy and matter radius. The calculated ground-state energy was 0.952 MeV and the rms radius was 2.46 fm (assuming a rms radius of 1.47 fm for the α particle). Both Coulomb and nuclear potentials are included. The fragment-target interactions were represented by optical potentials that reproduce the elastic scattering at the appropriate energy. The n + ^{120}Sn potential was taken from the global parametrization of Koning and

TABLE II. Total reaction cross sections for the ^{6}He + ^{120}Sn system obtained from the OM and CDCC calculations. The fourth column is the average between the second and third columns (see text for more details).

E (MeV)	$\sigma_{\rm reac}^{\rm OM}$ (mb)	$\sigma_{\rm reac}^{\rm CDCC}$ (mb)	$\sigma_{\rm reac}^{\rm av}$ (mb)	$\sigma^{\rm halo}$ (mb)	$\sigma_{\rm fus} = \sigma_{\rm reac}^{\rm av} - \sigma^{\rm halo}$ (mb)	$\sigma_{\rm fus}^{\rm Bass}$ (mb)
17.40	1451	1491	1471	768	703	618
18.05	1445	1592	1519	763	756	703
19.80	1475	1834	1655	739	916	900
20.50	1579	1916	1748	762	986	1065

Delaroche [24] and the α + ^{120}Sn potential was from the global parametrization of Avrigeanu *et al.* [25].

The coupled-channels equations were solved using the code FRESCO [13], which reads the coupling potentials externally. We included in the calculation the states with angular momentum $j = 0^{+}$, 1^{-}, and 2^{+}. To get convergence we needed a THO basis with 86 states up to a maximum energy value of 8 MeV.

Figure 3 shows the four-body CDCC calculations for the ^{6}He + ^{120}Sn at the different incident energies, $E_{\rm lab} = 17.40$, 18.05, 19.80, and 20.50 MeV, denoted by solid lines. The calculations reproduce quite well the data at the different energies. It is worth noting that there is no free parameter to adjust the calculation to the experimental data.

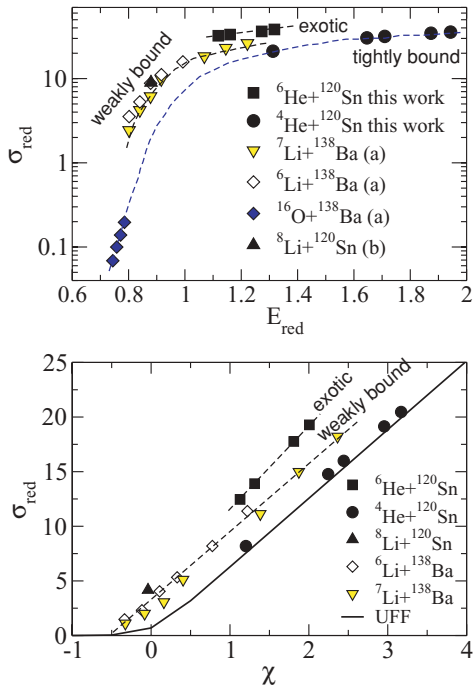

FIG. 4. (Color online) Reduced reaction cross section versus reduced energy for the ^{6}He + ^{120}S reaction compared to other systems of similar masses: (a) from Refs. [26,27] and (b) from Ref. [28]. The dashed lines are to guide the eyes. The total reaction cross sections were obtained from optical model fits of the experimental angular distributions. For the ^{6}He + ^{120}Sn system, we plot the average values of OM and four-body CDCC calculations from Table II. The upper and lower parts of Fig. 4 report the same data reduced by two different methods (see text for details).

C. The total reaction cross section

In Table II we compare the total reaction cross sections obtained from the OM and four-body CDCC calculations. The total reaction cross sections calculated with four-body CDCC are systematically about 10% larger than the OM results.

To compare the reaction cross section of different systems at different energies we make the transformation $\sigma_{\rm red} = \sigma_{\rm reac}/(A_p{}^{1/3} + A_t{}^{1/3})^2$ and $E_{\rm red} = E_{\rm cm}(A_p{}^{1/3} + A_t{}^{1/3})/Z_pZ_t$, where Z_p (Z_t) and A_p (A_t) are the charge and mass of the projectile (target), respectively. This procedure accounts for the geometrical effect in the cross section due to the size of the system and the effect of the Coulomb barrier. In the upper part of Fig. 4 we present the reduced reaction cross section versus the reduced energy for several systems with targets of masses around the ^{120}Sn mass. Angular distributions for the ^{4}He + ^{120}Sn system could also be measured in the present experiment due to the α contamination beam and were analyzed using the OM to obtain the reaction cross section plotted in Fig. 4 as solid circles. In the lower part of Fig. 4 we use the new prescription from Ref. [6], $\sigma'_{\rm red} = \frac{2E}{\hbar\omega R_B^2}\sigma$ and $\chi = \frac{E-E_B}{\hbar\omega}$ where R_B, E_B, and $\hbar\omega$ are respectively the radius, energy, and curvature of the Coulomb barrier. In Fig. 4, UFF stands for the universal fusion function [6].

We see that with both reduction methods, the ^{6}He + ^{120}Sn system presents the largest reaction cross section.

From this plot one can estimate the difference between the reduced reaction cross section for the ^{6}He + ^{120}Sn and the core ^{4}He + ^{120}Sn by calculating: $\sigma^{\rm halo} = [\sigma_{\rm red}^{^{6}{\rm He}+^{120}{\rm Sn}} - \sigma_{\rm red}^{^{4}{\rm He}+^{120}{\rm Sn}}] \times (A_p^{1/3} + A_t^{1/3})^2$. This difference is calculated at the same reduced energy. Since the ^{4}He projectile is the double-magic core of the ^{6}He, the only important reaction channels in $\sigma_{\rm red}^{^{4}{\rm He}+^{120}{\rm Sn}}$ should be the fusion and some inelastic excitation of the target. Thus $\sigma^{\rm halo}$ must represent the total contribution due to the projectile breakup + neutron transfer reactions + incomplete fusion processes. In Table II we present $\sigma^{\rm halo}$ obtained at the four energies measured. It is interesting to observe that $\sigma^{\rm halo}$ exhausts about one half of the total reaction cross section. The other half should be due to complete fusion and the difference $\sigma_{\rm fus} = \sigma_{\rm reac}^{\rm av} - \sigma^{\rm halo}$ (see Table II) agrees very well with complete fusion calculations for the ^{6}He + ^{120}Sn reaction using the Bass model [29].

IV. CONCLUSIONS

The first experimental data of the ^{6}He + ^{120}Sn scattering at energies near the Coulomb barrier are presented. The OM analysis of the angular distributions indicates the presence of a long-range imaginary potential. Four-body and three-body

CDCC calculations, considering the ^{6}He breakup channel, have been found to reproduce quite well the elastic angular distributions considering the experimental error bars.

The total reaction cross sections obtained from OM and four-body CDCC calculations for the ^{6}He + ^{120}Sn have been compared with other stable and exotic systems from the literature and the results show an enhancement of the total reaction cross section for the ^{6}He + ^{120}Sn system compared with other weakly bound and tightly bound projectiles. The contribution of the direct channels to the total reaction cross section was estimated from the scaled plot and was found to be of the order of one half of the total reaction cross section in the energy range of the data.

ACKNOWLEDGMENTS

The authors thank the Fundação de Amparo à Pesquisa do Estado de São Paulo (FAPESP) and the Conselho Nacional de Desenvolvimento Científico e Tecnológico (CNPq) for financial support. This work has been partially supported by the Complementary Action PCI2006-A7-0654, funded by the Spanish Ministry of Education and Science. A.M.M. and M.R.G. acknowledge the support by the Spanish Ministerio de Ciencia e Innovación under Project FPA2006-13807-c02-01, the local government of Junta de Andalucia under the Excellence Project P07-FQM-02894, and the Spanish Consolider-Ingenio 2010 Programme CPAN (CSD2007-00042).

[1] E. F. Aguilera *et al.*, Phys. Rev. Lett. **84**, 5058 (2000); Phys. Rev. C **63**, 061603(R) (2001).
[2] N. Keeley, J. M. Cook, K. W. Kemper, B. T. Roeder, W. D. Weintraub, F. Marechal, and K. Rusek, Phys. Rev. C **68**, 054601 (2003).
[3] O. R. Kaluee *et al.*, Nucl. Phys. A **728**, 339 (2003).
[4] K. Rusek, I. Martel, J. Gomez-Camacho, A. M. Moro, and R. Raabe, Phys. Rev. C **72**, 037603 (2005); K. Rusek, N. Keeley, K. W. Kemper, and R. Raabe, *ibid.* **67**, 041604(R) (2003).
[5] P. R. S. Gomes *et al.*, Phys. Lett. B **601**, 20 (2004).
[6] J. M. B. Shorto *et al.*, Phys. Lett. B **678**, 77 (2009).
[7] E. F. Aguilera *et al.*, Phys. Rev. C **79**, 021601(R) (2009).
[8] T. Matsumoto, E. Hiyama, K. Ogata, Y. Iseri, M. Kamimura, S. Chiba, and M. Yahiro, Phys. Rev. C **70**, 061601(R) (2004).
[9] M. Rodríguez-Gallardo, J. M. Arias, J. Gomez-Camacho, R. C. Johnson, A. M. Moro, I. J. Thompson, and J. A. Tostevin, Phys. Rev. C **77**, 064609 (2008).
[10] P. Descouvemont (private communication).
[11] R. Lichtenthäler *et al.*, Eur. Phys. J. A **25**, 733 (2005); Nucl. Phys. News **15**, 25 (2005).
[12] E. A. Benjamim *et al.*, Phys. Lett. B **647**, 30 (2007).
[13] I. J. Thompson, Comput. Phys. Rep. **7**, 167 (1988).
[14] P. R. S. Gomes *et al.*, Phys. Rev. C **71**, 034608 (2005).
[15] M. S. Hussein, P. R. S. Gomes, J. Lubian, and L. C. Chamon, Phys. Rev. C **73**, 044610 (2006).
[16] N. Austern *et al.*, Phys. Rep. **154**, 125 (1987).
[17] M. Takashina, S. Takagi, Y. Sakuragi, and Y. Iseri, Phys. Rev. C **67**, 037601 (2003).
[18] A. M. Moro, K. Rusek, J. M. Arias, J. Gomez-Camacho, and M. Rodriguez-Gallardo, Phys. Rev. C **75**, 064607 (2007).
[19] J. M. Lohr and W. Haeberli, Nucl. Phys. A **232**, 381 (1974).
[20] S. L. Tabor, B. A. Watson, and S. S. Hanna, Phys. Rev. C **11**, 198 (1975).
[21] M. Rodríguez-Gallardo, J. M. Arias, J. Gomez-Camacho, A. M. Moro, I. J. Thompson, and J. A. Tostevin, Phys. Rev. C **72**, 024007 (2005).
[22] I. J. Thompson, F. M. Nunes, and B. V. Danilin, Comput. Phys. Commun. **161**, 87 (2004).
[23] I. J. Thompson (unpublished; user's manual available from the author).
[24] A. J. Koning and J. P. Delaroche, Nucl. Phys. A **713**, 231 (2003).
[25] V. Avrigeanu, P. E. Hodgson, and M. Avrigeanu, Phys. Rev. C **49**, 2136 (1994).
[26] A. M. M. Maciel *et al.*, Phys. Rev. C **59**, 2103 (1999).
[27] C. P. Silva *et al.*, Nucl. Phys. A **679**, 287 (2001).
[28] P. N. de Faria, Ph.D. thesis, IFUSP, 2009.
[29] R. Bass, Phys. Rev. Lett. **39**, 265 (1977).